Water Depletion in the Disk Atmosphere of Herbig AeBe Stars

Fedele, D.; Pascucci, I.; Brittain, S.; Kamp, I.; Woitke, P.; Williams, J. P.; Dent, W. R. F.; Thi, W. -F.

Published in:
Astrophysical Journal

DOI:
10.1088/0004-637X/732/2/106

Publication date:
2011

The Astrophysical Journal, 732:106 (12pp), 2011 May 10 doi:10.1088/0004-637X/732/2/106

WATER DEPLETION IN THE DISK ATMOSPHERE OF HERBIG AeBe STARS*

D. Fedele[1], I. Pascucci[1,2], S. Brittain[3], I. Kamp[4], P. Woitke[5,6,7], J. P. Williams[8], W. R. F. Dent[9], and W.-F. Thi[10]
[1] Department of Physics and Astronomy, Johns Hopkins University, 3400 North Charles Street, Baltimore, MD 21218, USA; dfedele@pha.jhu.edu
[2] Space Telescope Science Institute, 3700 San Martin Drive, Baltimore, MD 21218, USA
[3] Department of Physics and Astronomy, Clemson University, Clemson, SC 29634, USA
[4] Kapteyn Astronomical Institute, Postbus 800, NL-9700 AV Groningen, The Netherlands
[5] Department of Astronomy, University of Vienna, Türkenschanzstr. 17, A-1180 Vienna, Austria
[6] SUPA, School of Physics & Astronomy, University of St. Andrews, North Haugh, St. Andrews KY16 9SS, UK
[7] UK Astronomy Technology Centre, Royal Observatory, Edinburgh, Blackford Hill, Edinburgh EH9 3HJ, UK
[8] Institute for Astronomy, University of Hawaii, 2680 Woodlawn Drive, Honolulu, HI 96822, USA
[9] ALMA JAO, Santiago, Chile
[10] UJF-Grenoble 1/CNRS-INSU, Institut de Plantologie et d'Astrophysique de Grenoble (IPAG) UMR 5274, F-38041 Grenoble, France
Received 2010 December 13; accepted 2011 March 9; published 2011 April 25

ABSTRACT

We present high-resolution ($R \sim 100{,}000$) *L*-band spectroscopy of 11 Herbig AeBe stars with circumstellar disks. The observations were obtained with the VLT/CRIRES to detect hot water and hydroxyl radical emission lines previously detected in disks around T Tauri stars. OH emission lines are detected toward four disks. The OH $^2\Pi_{3/2}$ P4.5 (1+,1−) doublet is spectrally resolved as well as the velocity profile of each component of the doublet. Its characteristic double-peak profile demonstrates that the gas is in Keplerian rotation and points to an emitting region extending out to ∼15–30 AU. The OH emission correlates with disk geometry as it is mostly detected toward flaring disks. None of the Herbig stars analyzed here show evidence of hot water vapor at a sensitivity similar to that of the OH lines. The non-detection of hot water vapor emission indicates that the atmospheres of disks around Herbig AeBe stars are depleted of water molecules. Assuming LTE and optically thin emission we derive a lower limit to the OH/H_2O column density ratio >1–25 in contrast to T Tauri disks for which the column density ratio is 0.3–0.4.

Key words: astrochemistry – molecular processes – protoplanetary disks – stars: pre-main sequence – stars: variables: T Tauri, Herbig Ae/Be

Online-only material: color figures

1. INTRODUCTION

Young pre-main-sequence stars (PMSs) are surrounded by gas-rich dust disks that are left over from the collapse of the molecular cloud core. Sub-micron-sized dust grains grow to larger sizes with time (e.g., Bouwman et al. 2001; Rodmann et al. 2006). This leads to the formation of planetesimals and eventually planets (e.g., Weidenschilling & Cuzzi 1993; Henning et al. 2006; Blum & Wurm 2008). The evolution of the infrared excess in PMSs suggests that most of the small dust grains in the disk disappear within 3–5 Myr from the collapse of the molecular cloud and only a very small amount of dust is found beyond 10 Myr (e.g., Haisch et al. 2001; Bouwman et al. 2006; Hernández et al. 2007; Roccatagliata et al. 2009; Pascucci & Tachibana 2010). A similar timescale is found for the evolution of mass accretion rates in disks (e.g., Mohanty et al. 2005; Jayawardhana et al. 2006; Sicilia-Aguilar et al. 2006; Ingleby et al. 2009; Fedele et al. 2010). The energetic radiation field of a PMS star impinging onto the disk surface regulates the disk temperature, can ionize the gas, breaks molecular bonds, and might lead to evaporation of the outer layers of the disk. Water plays an important role in the formation of a planetary system as well as in the origin of life on Earth. Compared to other volatiles (e.g., NH_3, CO_2, CH_4), water has a higher condensation temperature. Thus, within a protoplanetary disk, water is the first volatile to condense as temperature decreases as a function of the radial distance from the star and vertical depth. In view of the cosmic abundance of hydrogen and oxygen, water is the most abundant ice. This sets a boundary (*snow line*) beyond which most of the molecular gas condenses onto ice. For a review on the snow line in the solar nebula and in protoplanetary disks see, e.g., Podolak (2010). Beyond the snow line the solid surface density, and perhaps even the total surface density of the disk, increases (Kennedy & Kenyon 2008). This, in turn, speeds up the formation of gas giant planets allowing them to form before the gas in the disk is dispersed.

Water and hydroxyl (OH) emission have been detected in a number of protoplanetary disks around young sun-like stars in the near-infrared (Carr et al. 2004; Thi & Bik 2005; Salyk et al. 2008; Mandell et al. 2008) as well at mid-infrared wavelengths (10–40 μm) (Carr & Najita 2008; Salyk et al. 2008; Najita et al. 2010; Pontoppidan et al. 2010), and in the far-infrared with the *Herschel Space Observatory* (Sturm et al. 2010; van Kempen et al. 2010). Lines at different wavelengths trace different temperatures and hence different regions of the disk. While the near- to mid-infrared and high excitation far-infrared lines probe the molecular gas from the warm surface layers of the disk, the low excitation far-infrared lines are sensitive to colder gas (a few 100 K) located closer to the disk midplane (e.g., Woitke et al. 2009).

Mandell et al. (2008) performed high-resolution ($R \sim 27{,}000$) *L*-band spectroscopy toward two Herbig AeBe stars (AB Aur and MWC 758). They did not find evidence of hot water vapor emission in these two disks. Pontoppidan et al. (2010) searched for colder molecular emission in the mid-infrared using the *Spitzer Space Telescope*. In contrast to T Tauri stars, the mid-infrared spectrum of Herbig AeBe stars is poor in

* Based on observations collected at the European Southern Observatory, Paranal, Chile (Proposal ID: 082.C-0491).

Table 1
CRIRES Observation Log

Star	R.A. (J2000)	Decl. (J2000)	Observation Date	Exposure(s)	Air Mass	Calibrator
UX Ori	05:04:29.9	−03:47:11.1	2008 Dec 6; 02:50:50	1440	1.2	HD 36512
HD 34282	05:16:00.5	−09:48:31.2	2008 Dec 6; 01:47:50	1440	1.1	HD 40494
CO Ori	05:27:37.8	+11:25:33.3	2008 Dec 7; 04:32:54	720	1.2	HD 64503
V380 Ori	05:36:25.0	−06:43:00.3	2008 Dec 5; 02:36:08	720	1.4	HD 23466
BF Ori	05:37:12.9	−06:35:07.5	2008 Dec 7; 05:15:18	2400	1.1	HD 64503
HD 250550	06:01:59.5	+16:30:50.7	2008 Dec 6; 05:34:49	1080	1.3	HD 41753
HD 45677	06:28:17.3	−13:03:18.2	2008 Dec 6; 07:31:57	1080	1.1	HD 74195
HD 259431	06:33:04.6	+10:19:16.6	2008 Dec 6; 06:22:57	1080	1.2	HD 74280
HD 76534	08:55:08.6	−43:28:01.1	2008 Dec 5; 07:04:53	2400	1.1	HD 28873
HD 85567	09:50:28.2	−60:58:02.9	2008 Dec 6; 08:22:59	480	1.3	HD 98718
HD 98922	11:22:31.0	−53:22:07.9	2008 Dec 5; 08:19:43	720	1.3	HD 39764

molecular emission and they find only tentative H_2O and OH emission lines toward some Herbig AeBe stars.

The different molecular emission between T Tauri and Herbig AeBe stars might be due to the photochemistry which controls the excitation and dissociation of molecules. Aiming to test this hypothesis, we performed a deep search for hot water and hydroxyl radical vapor emission in Herbig AeBe stars with circumstellar disks. We performed ultra high-resolution ($R \sim 100{,}000$, $\Delta v \sim 3$ km s^{-1}) L-band spectroscopy of 11 Herbig AeBe stars with CRIRES at the VLT. This spectral resolution allows us to resolve the velocity profile of the molecular emission lines and thus determine the radii over which the emission arises.

Observations and data reduction procedures are presented in Section 2. In Section 3, we describe the immediate results of the survey: the detection of the OH $^2\Pi_{3/2}$ P4.5 (1+,1−) rovibrational line and the non-detection of water rovibrational lines. In Section 4, we present the analysis of the OH lines and discuss the implications of our findings in Section 5. Finally, we summarize our results in Section 6.

2. OBSERVATIONS AND DATA REDUCTION

High-resolution L-band spectroscopy was obtained on the nights of 2008 December 4, 5, and 6 with the ESO's VLT cryogenic high-resolution infrared echelle spectrograph (CRIRES; Kaeufl et al. 2004) at the Paranal observatory in Chile. A slit width of 0.″2 was adopted. In order to center the target inside the narrow slit, we used the adaptive optics system and the targets themselves as reference stars. This procedure reduces slit losses resulting in a higher signal-to-noise ratio and higher spectral resolution. Unresolved sky emission lines can be used to determine the actual spectral resolution. The full width at half-maximum (FWHM) of the OH sky lines measured in the raw frames is ∼3 km s^{-1} (or $R \sim 100{,}000$) as expected from the nominal resolution. The spectra were recorded by nodding the telescope along the direction perpendicular to the slit (oriented along the parallactic angle) with a nodding throw of 10″. The spectra cover the wavelength range between 2861 and 2936 nm (order 19, $\lambda_{\rm ref} = 2909.6$ nm) thus covering several rovibrational lines of H_2O detected in comets (e.g., Dello Russo et al. 2004, 2005) and in protoplanetary disks (Salyk et al. 2008) as well as rovibrational lines of OH detected in disks by Mandell et al. (2008) and Salyk et al. (2008).

The data were reduced using the ESO CRIRES pipeline v.11.0[11] following a standard approach: first the CRIRES frames are corrected for flat field, dark, and bad pixels; second the frames at a given nodding position are combined together and the two master frames (one for each nodding position) are then combined together after correcting for the spatial offsets (due to the nodding procedure); finally, the spectrum is extracted using a rectangular mask. The sky emission lines are used to determine the wavelength dispersion solution. To properly correct for atmospheric telluric absorptions, the spectra were bracketed with observations of standard stars of early spectral type (see Table 1). These spectra are divided by the stellar atmosphere models of Kurucz (1979) to determine the instrument response function and atmospheric transmission curve. The optical depth of the telluric lines is scaled to the depth of the science target. Finally, each science spectrum is divided by the response function. The spectral regions heavily absorbed (atmospheric transmission <0.5) are not used in the rest of the analysis. For the flux calibration, we scaled the CRIRES spectra to the observed L-band magnitude measured by de Winter et al. (2001; V380 Ori, HD 76534, UX Ori, HD 250550, HD 259431, HD 45677, BF Ori), Malfait et al. (1998; HD 98922, HD 34282, HD 85567), and Morel & Magnenat (1978; CO Ori).

Given the high temperatures of the stellar photosphere of Herbig AeBe stars, the L-band spectrum is relatively free of stellar photospheric absorption lines. The spectra of all the stars observed with CRIRES are continuum dominated and have high signal-to-noise ratio (S/N > 100). Such a high ratio allows the detection of weak emission lines down to a few percent of the continuum flux level. The exposure times vary from object to object and range from ∼10 minutes (for targets of $L \sim 4-6$ mag) to 40 minutes ($L \sim 7$ mag). The log of the observations is given in Table 1.

3. IMMEDIATE RESULTS

We have searched for H_2O and OH rovibrational lines previously detected in protoplanetary disks around sun-like stars, comets, as well as transitions that are not yet detected but reported in recent synthetic molecular line lists. In the following section, we summarize the main findings for H_2O and OH.

3.1. Detection of OH Lines

The rovibrational OH $^2\Pi_{3/2}$ P4.5 (1+,1−) at 2.9345 μm transition is detected toward four disks (V380 Ori, HD 250550, HD 259431, and HD 85567; Figure 1). The high spectral resolution of CRIRES allows us to resolve not only the doublet but also the velocity profile of each transition. Modeling of the line profiles and estimates of the radii traced by this emission are presented in Section 4.

[11] http://www.eso.org/sci/software/pipelines/

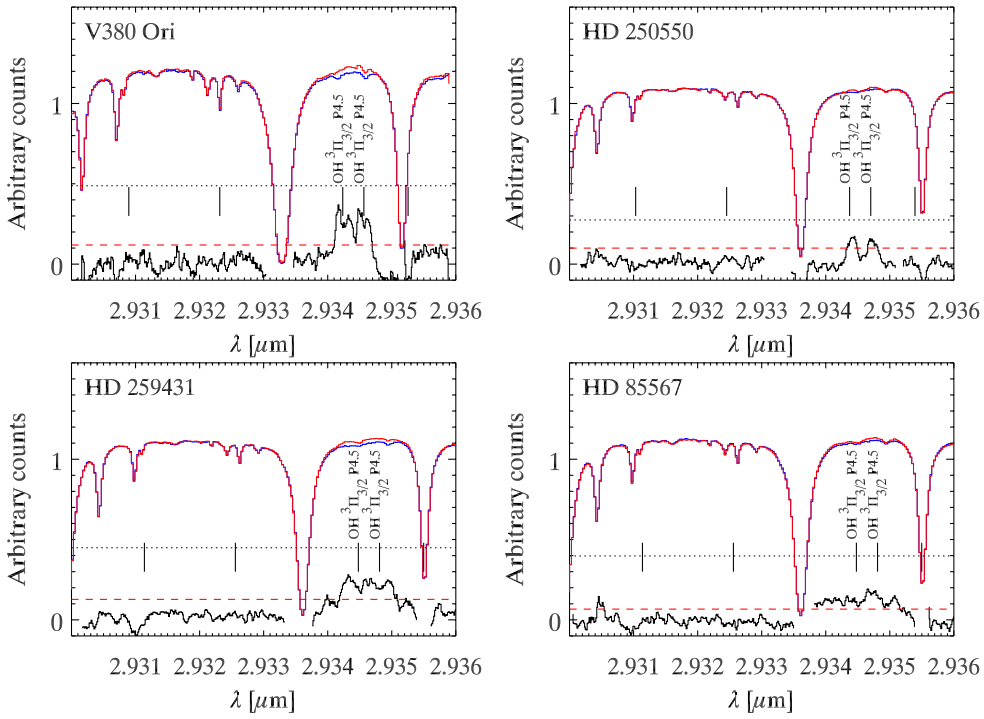

Figure 1. Portion of the CRIRES spectra for V380 Ori, HD 250550, HD 259431, and HD 85567. In each panel, the upper line (red) is the extracted target spectrum along with the atmospheric transmission curve (blue line). The lower plot of each frame is the spectrum cleaned by the telluric absorption lines multiplied by a factor of 10. The dashed line shows the 3σ detection level. For each star, the OH P4.5 (1+,1−) doublet is detected and spectrally resolved. The vertical lines show the positions of some of the strongest H_2O rovibrational lines. The dotted line indicates the expected line height of the H_2O (001–000) [11_{66}–12_{67}] transition in the case of an OH/H_2O column density ratio equal to unity.

(A color version of this figure is available in the online journal.)

The profile of the $^2\Pi_{3/2}$ P4.5 (1+,1−) line varies from object to object (Figures 2–5). In the case of V380 Ori each line shows a characteristic double-peak profile as one would expect if the gas is in Keplerian rotation. In the case of HD 250550, the lines are narrower reflecting the lower inclination of the disk. Finally, the OH line in HD 259431 and HD 85567 is very broad and the two transitions of the doublet are blended even at the high resolution of CRIRES. In the case of HD 259431, multiple peaks are visible hinting at multiple velocity components. Two peaks are detected (above 3σ) at the sides of the line at 2.9340 μm and 2.9352 μm, respectively. The positions of these peaks are symmetric about the center of the emission and correspond to a velocity of ± 47 km s^{-1}. The OH emission is very broad (FWHM = 90 km s^{-1}) and the sides of the emission might be contaminated by the strong telluric absorptions at 2.9335 μm and 2.9355 μm. We used different telluric standard stars (taken at different air mass) to check the reliability of the line profile. In all cases, we found the two high-velocity wings above the 3σ level. Further confirmation of the presence of these wings comes from an a posteriori analysis of the line profile (Section 4.2): if the OH emission is made of a single velocity component, the central part of the emission would be stronger than the sides due to the blending of the line (see e.g., the dot-dashed line in Figure 5). The analysis of the line profile confirms the presence of multiple velocity components and the reliability of the high-velocity peaks. At higher velocity, where the atmospheric transmission function drops below 70%, the emission is heavily corrupted by telluric absorption; hence we excluded these regions from the analysis of the line.

Within the spectral range covered by our observations there are other two transitions of the OH $^2\Pi_{3/2}$ P branch (J = 2.5, 3, 5) as well as two transitions of the OH $^2\Pi_{1/2}$ P branch (J = 2.5, 3.5). Unfortunately all four transitions fall either in highly saturated telluric absorption regions or inside the inter-chips gaps; hence we cannot compute stringent upper limits on the line flux.

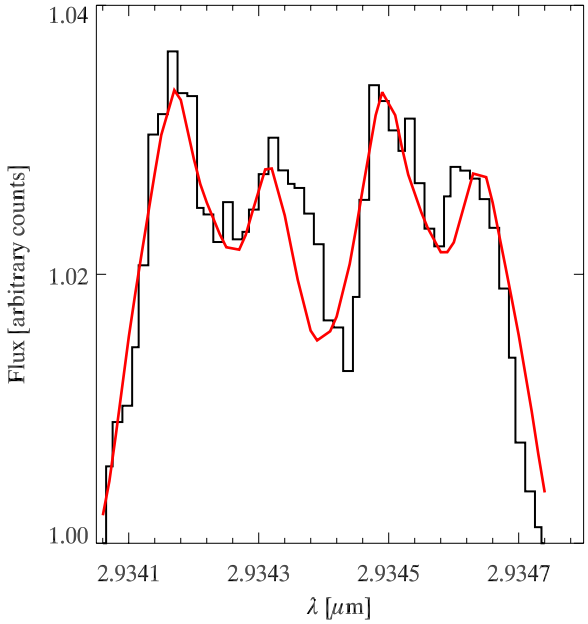

Figure 2. OH P4.5 doublet toward V380 Ori. The red line is the best-fit model (Section 4.2, Table 4) assuming Keplerian rotation. The asymmetry of the line profile indicates a deviation from the Keplerian motion of the gas (see the Appendix).

(A color version of this figure is available in the online journal.)

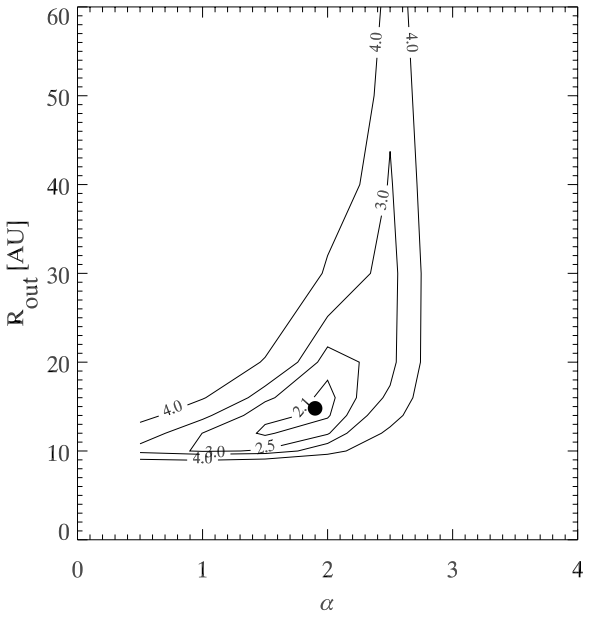

Figure 3. $\tilde{\chi}^2$ contours in the α–R_o parameter space for V380 Ori assuming $i = 30^\circ$ and $R_i = 2$ AU. The best-fit value is shown as a black dot.

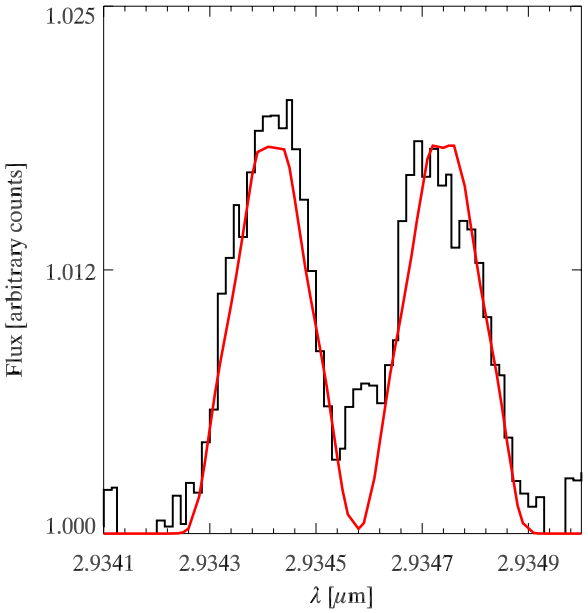

Figure 4. Same as Figure 2 for HD 250550.
(A color version of this figure is available in the online journal.)

3.1.1. OH Column Density

The energy level of the rovibrational transitions of OH might be populated either thermally or radiatively (fluorescence). In the first case, the collisions with atoms and molecules are the dominant excitation mechanism and the emission is only dependent on the temperature and density of the gas as we will show below (LTE case). In the case of fluorescent emission, the rovibrational levels are populated by absorption of near-infrared photons (in the electronic ground state) or absorption of UV photons which excite the electronic states with a following cascade in the electronic ground state. UV fluorescent pumping in protoplanetary disks was investigated for the first time by Brittain et al. (2003, 2007) to explain the CO emission from the disk around the HAeBe stars HD 141569 A and AB Aur.

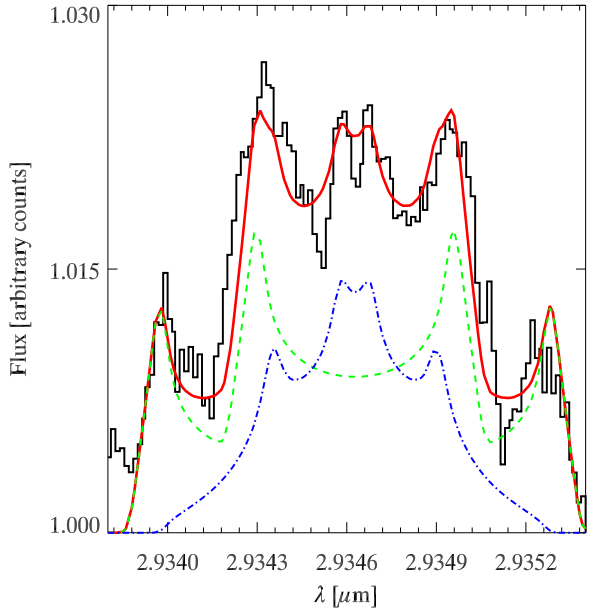

Figure 5. Same as Figure 2 for HD 259431. The dashed and dot-dashed lines are the the optically thick and disk's atmosphere components, respectively.
(A color version of this figure is available in the online journal.)

Mandell et al. (2008) implemented UV and IR fluorescent pumping for the OH rovibrational lines detected in the disk around AB Aur and MWC 758. They found that a fluorescent model can explain the observed OH line intensities as well as OH thermal emission. The difference between thermal and fluorescent emission is in the inferred OH column densities, which are higher in the LTE case. Since our observations do not allow us to discriminate between LTE and fluorescent emission, we assume in the following analysis that the OH gas is in LTE, the emission is optically thin, and compute the total number of OH molecules from the measured line flux. For the gas temperature, we take a value of 700 K as estimated by Mandell et al. (2008) for the Herbig AeBe stars AB Aur and MWC 758. With these assumptions, the OH line intensity is (Herzberg 1950)

$$I(\mathrm{OH}) = N_n(\mathrm{OH}) h \tilde{\nu} c A_{nm} \quad (1)$$

with I(OH) the OH line luminosity ($= 4\,\pi d^2 F_{\mathrm{OH}}\, d$ with the distance to the star and F_{OH} the measured OH flux), N_n the number of molecules in the upper state n, h is Planck's constant, c is the velocity of light, $\tilde{\nu}$ the wavenumber of the transition (cm^{-1}), and A_{nm} the Einstein coefficient of the $^2\Pi_{3/2}$ P4.5 transition. In LTE, the quantity N_n relates to the total number of OH molecules (N) as

$$\frac{N_n(\mathrm{OH})}{N(\mathrm{OH})} = \frac{g_J \exp(-E_n/kT)}{Q(T)}, \quad (2)$$

where g_J ($= 2J + 1$) is the degeneracy of the state, E_n the energy of the upper state, k the Boltzmann constant, and $Q(T)$ the partition sum. Substituting N_n from Equation (2) in Equation (1), we have

$$N(\mathrm{OH}) = \frac{I(\mathrm{OH}) Q(T) \exp(E_n/kT)}{hc\tilde{\nu} A_{nm}(2J+1)}. \quad (3)$$

The transition parameters and the partition sum are taken from HITRAN (Rothman et al. 2009). The total number of molecules can be converted into a vertical column density

($N_{\rm col}$) by dividing it by the area of the OH emitting region, $\pi(R_o^2 - R_i^2)$, with R_i and R_o being the inner and outer radii of the OH emitting region (see Section 4.2). When the OH P4.5 doublet is not detected and the emitting region is not known, we assume $R_i = 0.4$ AU and $R_o = 10$ AU and a line width of 30 km s^{-1} (based on our results for the OH line detections). The values of N and $N_{\rm col}$ are listed in Table 3. We note that increasing the temperature to T(OH) = 1000 K decreases N (hence $N_{\rm col}$) by almost an order of magnitude.

3.2. Non-detection of H_2O Lines

In order to search for faint water vapor emission, we first created a line list using the water line list catalog of Barber et al. (2006). The latter is the most complete and accurate water line list in the literature. We used their *BT2* code to produce the synthetic spectrum and adopted the same temperature as that for the OH gas (700 K). Some of the strongest water lines detected by Salyk et al. (2008) in the T Tauri stars AS 205 A and DR Tau lie around 2930 nm, close to the OH $^2\Pi_{3/2}$ P4.5 doublet we have detected in 4 disks and hence in a clean part of the spectrum. For comparison, Figure 1 shows the positions of the strongest water emission lines from Salyk et al. (2008). None of the 11 Herbig AeBe stars observed with CRIRES show evidence of hot water vapor emission in the *L*-band spectra.

We compute the 3σ upper limit of the line flux for the line H_2O (001–000) [11_{66}–12_{67}] at 2.931 μm detected in T Tauri stars. The upper limit is measured as the product $3 \times \sigma \times \Delta\lambda$, where σ is the standard deviation of the spectrum and $\Delta\lambda$ is a characteristic line width of 30 km s^{-1} or 2.9×10^{-4} μm (of the same order as the OH line width). The line flux upper limits for the program stars are given in Table 3. Typical upper limits are of the order of 10^{-16} to 10^{-15} erg cm^{-2} s^{-1}. The water lines detected by Salyk et al. (2008)[12] have fluxes of the order of 10^{-15} to 10^{-14} erg cm^{-2} s^{-1}.

3.2.1. H_2O Column Density

With the same assumptions as Section 3.1.1 (optically thin emission, LTE, $T = 700$ K), we can estimate the upper limit on the total number of molecules and the column density of H_2O. In the case of water, Equation (3) must be modified to take into account an additional degeneracy associated with the nuclear spin ($g_{\rm I} = 3$ for J odd and $g_{\rm I} = 1$ for J even). We compute the upper limits of $N(H_2O)$ and $N_{\rm col}(H_2O)$ using the line flux upper limits of the (001–000) [11_{66}–12_{67}] transition. The results are listed in Table 3. We note that in this case also, the number of molecules decreases by almost an order of magnitude if the temperature is increased to $T(H_2O) = 1000$ K.

3.3. OH/H_2O Line Ratio

From the comparison of Figure 1 with Figure 2 of Salyk et al. (2008), it is evident that the OH/H_2O line ratio is higher in Herbig AeBe disks than in T Tauri disks. For the Herbig stars with detected OH emission lines, we have that the OH/H_2O line flux ratio is $\gtrsim 1.5 - 30$.[13] This translates into a lower limit on the OH/H_2O column density ratio of 1–25 (Table 3). For comparison, we show in Figure 1 the expected line height of the H_2O (001–000) [11_{66}–12_{67}] transition in the case of an OH/H_2O column density ratio equal to unity (dotted line). The intensity of the OH P4.5 line for the four Herbig AeBe stars (Table 3) is of the order of 10^{-15}–10^{-14} erg cm^{-2} s^{-1}, similar to the OH and H_2O line flux measured in T Tauri disks (Salyk et al. 2008). However, in the case of T Tauri disks, the OH/H_2O line flux ratio is ~1 and the column density ratio is 0.3–0.4, that is, the OH/H_2O column density ratio is ~3–25 times larger in Herbig AeBe disks than in T Tauri disks. This suggests that, in contrast to T Tauri disks, water vapor is less abundant than OH in the disk atmosphere of Herbig AeBe stars.

4. ANALYSIS

In order to understand the pattern of detections and non-detections, we investigate whether there is any correlation between stellar and disk properties and the surveyed emission lines (Section 4.1). We also model the profiles of the resolved OH lines and provide estimates for the radial distances traced by the *L*-band OH emission in disks around Herbig AeBe stars (Section 4.2).

4.1. OH Lines and Disk Properties

A noticeable distinction appears when detections are compared with the disk geometry: the majority of the sources with detection of OH emission appear to have a flared disk geometry. Meeus et al. (2001) have shown that the ratio of the far-infrared to the near-infrared flux is sensitive to the geometry of the disk. Far-infrared bright stars belonging to the group I of Meeus et al. (2001) are thought to have a flared disk geometry, that is the disk scale height (H) and opening angle (H/R) of the disk increases with the distance from the star (R). Group II sources are thought to have a flat, self-shadowed geometry, due to the disk inner rim casting a shadow at larger disk radii (Dullemond & Dominik 2004). van Boekel et al. (2003) found that the two groups occupy two different regions in the *IRAS* m_{12}–m_{60} color versus $L_{\rm NIR}/L_{\rm IR}$ diagram, where $L_{\rm NIR}$ is the integrated luminosity as measured by the *J, H, K, L,* and *M* photometry and $L_{\rm IR}$ is the integrated luminosity measured by the *IRAS* 12, 25, and 60 μm fluxes. Following van Boekel et al. (2003), we list in Table 2 the group of the program stars. Interestingly, three out of the four stars for which OH emission is detected (V380 Ori, HD 250550, HD 259431) belong to group I while only one source showing OH emission (HD 85567) belongs to group II. We note that the other two HAeBe stars with detected OH emission in the literature (AU Aur and MWC 758; Mandell et al. 2008) also belong to group I. We discuss the origin of such a correlation in Section 5.5.

4.2. OH Line Profiles

In this section, we present an analysis of the OH P4.5 (1+,1−) line profiles for V380 Ori, HD 250550, HD 259431, and HD 85567. Figures 2–5 show the velocity profile of the doublet for the four stars from which we can estimate the radial distribution of the molecular gas. We assume that the line intensity follows a power-law distribution as a function of the radial distance from the star (e.g., Smak 1981; Carmona et al. 2007; van der Plas et al. 2009) of the form

$$I_{\rm OH}(R) = I_{\rm OH}(R_0) \cdot (R/R_0)^{-\alpha}, \quad (4)$$

where R is the distance from the star and $I_{\rm OH}(R_0)$ is the intensity at the inner radius. We also assume that the OH line is optically thin. If the line is optically thick, we should include in the analysis the continuum and line optical depths (e.g., Horne & Marsh 1986). Here, we are interested in determining the

[12] Estimated from Figure 2 of Salyk et al. (2008).
[13] We refer here to the total flux of the OH P4.5 doublet, i.e., twice the value listed in the fourth column of Table 3.

Table 2
Properties of the Program Stars

Star	Sp. Type	Age (Myr)	A_V (mag)	D (pc)	L_{UV}[a] ($L_\odot$)	$\dot{M}_{acc}$ (10^{-7} $M_\odot$ yr^{-1})	Group
UX Ori	A3	4.5[b]	0.8[c]	460[d]	2.4	0.66[e]	II
HD 34282	A0	7[f]	0.6[c]	160[g]	...	<0.2[h]	I
CO Ori	F7	<0.12[c]	2.2[c]	460[d]	2.9[i]	0.9[j]	II
V380 Ori	A1	<0.01[c]	1.43[g]	430[d]	18.8	25[e]	I
BF Ori	A5	3.2[b]	0.37[k]-0.7[c]	460[d]	0.6-1.3	0.87[e]	II
HD 250550	B7	0.25[c]	1.17[c]	700[d]	160	0.16[e]	I
HD 45677	B2	...		>500[l]	>65		II
HD 259431	B5	<0.01[c]	0.63[k]-1.62[g]	800[d]	225-2200	7.8[e]	I
HD 76534	B2	$\gtrsim$0.5[m]	0.80[k]	870[d]	1020[n]		I
HD 85567	B5	<0.01[c]	2.23[c]	1500[c]	...		II
HD 98922	B9	<0.01[c]	0.54[c]	1000[c]	545	17.4[h]	II

Notes.
[a] Integrated between 1100 and 2430 Å (*IUE* spectrum; Valenti et al. 2003) and multiplied by a factor $10^{0.4 \cdot A_{1770}}$. Where A_{1770} is the extinction at $\lambda = 1770$ Å measured from A_V using the $R = 3.1$ extinction relation of Cardelli et al. (1989).
[b] Montesinos et al. (2009).
[c] Manoj et al. (2006).
[d] Hillenbrand et al. (1992).
[e] Donehew et al. (submitted).
[f] Merín et al. (2004).
[g] van den Ancker et al. (1998).
[h] Garcia Lopez et al. (2006).
[i] Missing short-wavelength *IUE* spectrum, integrated between 1850 and 2430 Å.
[j] Calvet et al. (2004).
[k] Valenti et al. (2003).
[l] de Winter & van den Ancker (1997).
[m] Martin-Zaïdi et al. (2008).
[n] Missing long-wavelength *IUE* spectrum, integrated between 1150 and 2000 Å.

Table 3
OH and H_2O Line Parameters[a]

Star	OH FWHM (km s^{-1})	OH |EW| (10^{-6} μm)	L_{OH} (10^{-15} erg cm^{-2} s^{-1})	L_{H_2O} @ 2.931 μm (10^{-15} erg cm^{-2} s^{-1})	log(N(OH)) (molecules)	log(N_{col}(OH)) (mol./cm^{-2})	log(N(H_2O)) (molecules)	log(N_{col}(H_2O)) (mol./cm^{-2})
UX Ori			<3.0		<44.3	<15.4	<44.3	<15.5
HD 34282			<2.0		<43.2	<14.3	<43.2	<14.4
CO Ori			<1.0		<43.8	<15.0	<43.9	<15.0
V380 Ori	27	8	8.4 (± 5.0)	<4.5	45.0	16.1	<44.5	<15.6
BF Ori			<1.0		<43.8	<15.0	<43.9	<15.0
HD 250550	18	2.8	1.4 (± 0.1)	<2.0	44.6	15.9	<44.5	<15.8
HD 45677			<10		<43.9	<15.0	<43.9	<15.1
HD 259431	45[b]	12	14.5 (± 2)	<1.0	45.7	15.9	<44.3	<14.5
HD 76534			<1.5		<44.5	<15.7	<44.6	<15.7
HD 85567	30[b]	8	10.0 (± 30)	<3.0	46.1	17.3	<45.4	<16.5
HD 98922			<1.2		<44.6	<15.7	<44.6	<15.8

Notes.
[a] Upper limits are computed as the product $3 \times \sigma \times \Delta\lambda$, with σ the standard deviation between 2.930 μm and 2.936 μm and $\Delta\lambda = 30$ km s^{-1}. The OH line flux refers to the average flux of the two transitions of the $^2\Pi_{3/2}$ P4.5 (1+,1−) doublet. The FWHM and EW are the mean of the FWHM and EW of the two transitions. Total and column densities are computed assuming optically thin emission, LTE and T(OH) = T(H_2O) = 700 K, respectively.
[b] In this case the OH doublet is blended (Figures 5 and 7). The FWHM and EW are computed as half of the total doublet FWHM and EW.

inner and outer radii of the OH emitting region and a complete analysis of the line emission properties is beyond the scope of this paper. The radial profile of the OH line is converted into a velocity profile assuming that the gas is in Keplerian rotation. In addition, the model line is convolved with a velocity width $v = \sqrt{v_{in}^2 + v_{th}^2}$, where v_{in} is the instrumental broadening (∼3 km s^{-1}) and v_{th} ($= \sqrt{2kT/m_{OH}}$) is the thermal broadening of the line (where k is the Boltzmann constant, T is the gas temperature, and m_{OH} is the mass of OH). We assume a temperature of 700 K as found by Mandell et al. (2008) which corresponds to $v_{th} \sim 0.8$ km s^{-1}. For the Keplerian rotation and line convolution, we used the IDL codes "keprot" and "convolve"[14] described in Acke et al. (2005).

With the assumption of Keplerian rotation and the radial profile in Equation (4), the velocity profile of the emission line is a function of four parameters: the power-law intensity exponent (α), the disk inclination (i), and the inner and outer radii

[14] http:www.ster.kuleuven.ac.be/∼bram/dark_theme/work.html

Table 4
Stellar and Disk Parameters

Parameters	V380 Ori	HD 250550	HD 259431[a]
M_* ($M_\odot$)	2.8[b]	3.6[c]	6.6[d]
i (°)	30–35	8–15	50[d]
α	2.0	2.5	0
R_i (AU)	2.0–2.1	0.4–0.7	0.8–1.0
R_o (AU)	12–16	100[e]	1.3–1.5
α_2			2.0
$R_{2,i}$ (AU)			1.3–1.5[f]
$R_{2,o}$ (AU)			23–30
$\tilde{\chi}^2$	1.9	1.2	1.4

Notes.
[a] In the case of HD 259431 the model is the sum of two velocity components. The subscript "2" refers to the second velocity component.
[b] Hubrig et al. (2009).
[c] Hernández et al. (2004).
[d] Kraus et al. (2008)
[e] Fixed.
[f] Constrained to be $\geqslant R_{1,o}$.

of the OH emitting region (R_i, R_o). The Keplerian velocity is $v_{\rm kep} = \sqrt{GM_*/R}$; hence the inner radius determines the maximum velocity in the line profile. Because the disk inclination is not known for our sources (apart from HD 259431), we fitted the OH P4.5 doublet by minimizing the reduced χ^2 ($\tilde{\chi}^2$) between the observed and model velocity profiles,

$$\tilde{\chi}^2 = \frac{1}{d}\sum\left(\frac{\text{model} - \text{observed}}{\sigma}\right)^2, \quad (5)$$

with d being the degrees of freedom. In our fitting procedure, we leave free only three parameters: i, R_i, and R_o and repeat the model fitting for five different values of α (0, 1.0, 1.5, 2, 2.5). The best-fit parameters are listed in Table 4.

4.2.1. Determination of the Outer Disk (R_o)

The measurement of R_o requires further explanation. The contribution from the outer disk to the line intensity is reduced because of the power-law distribution (Equation (4)). Moreover, the fit to the line profile might be degenerate if the parameters are not independent. As we saw above, R_i is uniquely determined by the maximum velocity of the line. In a Keplerian motion, the disk inclination and outer radius are responsible for the characteristic double-peak profile: for a given ring of gas at a distance R from the central star the two peaks of the line are separated by the quantity $v_{\rm kep} \cdot \sin(i) \propto R^{-1/2} \cdot \sin(i)$. If the disk inclination is known, it is possible to unambiguously determine R_o. The power-law index (α) controls how steeply the intensity decreases with radius (hence velocity) and affects only slightly the peak-to-peak separation as shown in Figure 1 of Smak (1981). To check the robustness of the fit we first determine the best-fit parameters, then we fix the disk inclination and inner radius and compute the $\tilde{\chi}^2$ surface on the α–R_o parameter space.

Notes on individual targets:

V380 Ori. The OH emission extends from ∼2 AU to ∼15 AU from the central star (Figure 2) and we estimate a disk inclination of ∼30°. Figure 3 shows the $\tilde{\chi}^2$ of the fit in the α–R_o plane. The single-peak $\tilde{\chi}^2$ distribution shows that the determination of R_o is robust. The OH P4.5 line profile is asymmetric with the blue peak stronger than the red peak. The model in Figure 2 has been manually modified to account for the excess flux in the blueshifted peak by multiplying the latter by a factor of 1.2. The origin of the asymmetric line profile is discussed in the Appendix.

HD 250550. In this case, the line is top flat and the two peaks are not visible. This is likely due to the low inclination of the disk in the plane of the sky (disk almost face-on). In this situation, it is not possible to determine R_o unambiguously so we fix it to a value of 100 AU. The best fit is found for an inner radius of ∼0.4 AU and an inclination of 10°.

HD 259431. The OH line profile in this case is more complicated and appears to have multiple components. We note that we were not able to fit the OH line profile with a model made of a single velocity component as in the previous cases. Multi-wavelength interferometric observations reveal the presence of optically thick gas within the dust sublimation radius (Kraus et al. 2008). In particular, the near-infrared continuum is dominated by optically thick gas that is accreting onto the star, while the mid-infrared continuum arises from the passively irradiated disk atmosphere at larger radii. Similarly, the analysis of the H_2 FUV lines (Bouret et al. 2003) suggests that the molecular hydrogen spectrum (seen in absorption) has multi-temperature components. In particular, they find that a hot component ($T \sim 1300$ K) comes from optically thick gas in the vicinity (>0.5 AU) of the star. This is in good agreement with the detection of the high-velocity wings in the OH line profile (Section 3). To account for the presence of optically thick gas inside the dust truncation radius we modify the standard model to include a second component (see Figure 5). Thus, the free parameters of the fit are now five: disk inclination, inner and outer radii of the optically thick component ($R_{1,i}$, $R_{1,o}$), and inner and outer radii of the passively irradiated disk component ($R_{2,i}$, $R_{2,o}$). We adopt a disk inclination of 50° based on the results of Kraus et al. (2008). For the thermal broadening of the line, we assume $T_1 = 1300$ K (=$T(H_2)$) and $T_2 = 700$ K (from Mandell et al. 2008) for the high- and low-velocity components, respectively. Finally, we assume a constant dependence of the line intensity on the radius ($\alpha = 0$ in Equation (4)) for the high-velocity component. Our best model parameters are in good agreements with the results of the interferometric observations: the first component extends from ∼0.8 AU to ∼1.4 AU and the second component extends from ∼1.4 AU to ∼25 AU from the star. We note that our fitting routine tends to produce a low value of $R_{2,i}$ (lower than $R_{1,o}$), thus we constrain $R_{2,i}$ to be $\gtrsim R_{1,o}$. Figure 6 shows the $\tilde{\chi}^2$ of the fit in the α–$R_{2,o}$ plane (after fixing all the other parameters). The value of $R_{2,o}$ is not degenerate with α.

Recently, Bagnoli et al. (2010) found a similar result for the [O I] line at 6300 Å. High spectral resolution observations revealed the presence of a high-velocity component between ∼1 and 2 AU and a low-velocity component peaking around 20 AU. Compared to the [O I] line profile, the OH high-velocity component is clearly double-peaked and allows us to constrain better the outer radius of the high-velocity component ($R_{1,o}$). Compared to the [O I] 6300 Å line, the OH emission detected here likely arises from deeper layers (higher A_V) in the disk.

HD 85567. The OH emission is broad (of the order of ∼100 km s^{-1}) and suggests the presence of high-velocity molecular gas. As in the case of HD 259431, the high-velocity OH emission might originate in an optically thick gas inside the dust sublimation radius. There are no estimates of the disk inclination in the literature and given the low S/N of the spectrum it is hard to estimate the radial extent of the OH

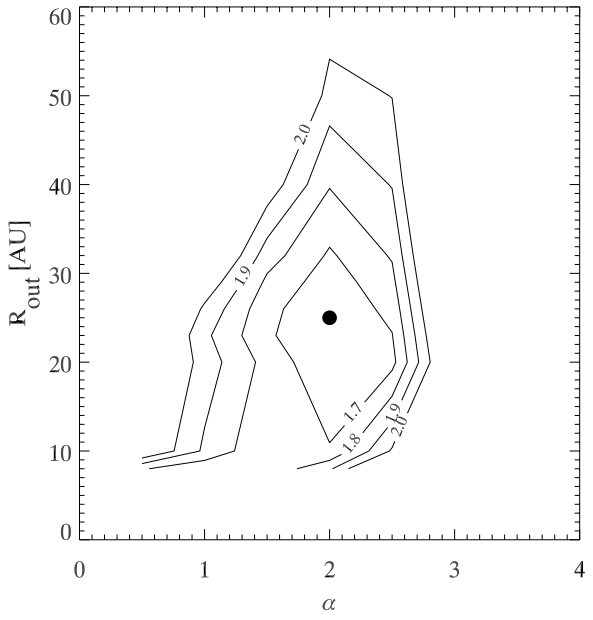

Figure 6. $\tilde{\chi}^2$ contours in the α_2–$R_{2,o}$ parameter space for HD 259431 assuming $i = 50°$, $\alpha_1 = 0$, $R_{1,i} = 0.9$ AU and $R_{1,o} = R_{2,i} = 1.4$ AU. The best-fit value is shown as a black dot.

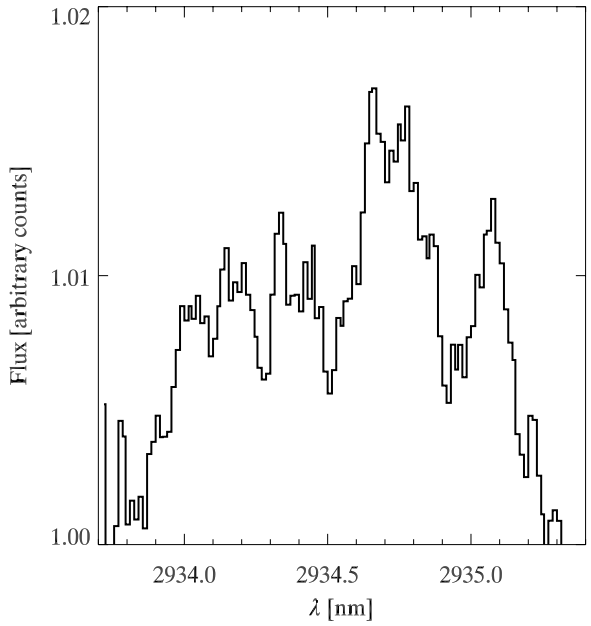

Figure 7. OH P4.5 doublet toward HD 85567.

emitting region. Further observations are needed to measure the properties of the OH emission from this disk.

5. DISCUSSION

The main findings of Sections 3 and 4 are: (1) the non-detection of water vapor emission lines, (2) the detection of OH emission lines from the disk atmosphere of Herbig AeBe stars, and (3) the correlation between OH emission and disk flaring. In contrast, observations of T Tauri stars have shown that a hot (500–1000 K) water layer exists in their disk atmosphere with densities similar to the OH layer we detect in Herbig AeBe stars (e.g., Carr & Najita 2008; Salyk et al. 2008). In this section, we discuss the processes affecting the formation and destruction of water molecules in disks. The discussion is structured as follow: first we explain how water molecules form in the disk atmosphere (Section 5.1); then we address the water (and OH) destruction processes and outline the main differences between T Tauri and Herbig AeBe stars (Section 5.2). Finally, we examine how non-stationary processes might affect the water content in different regions of the disk (Sections 5.3 and 5.4) with a final discussion on the origin of the OH disk geometry correlation (Section 5.5).

5.1. Formation of Water in Disks

The formation of water molecules in the warm disk atmosphere is a three-step process:

$$\mathrm{H + H + dust \rightarrow H_2 + dust} \quad (6)$$

$$\mathrm{O + H_2 \rightarrow OH + H} \quad (7)$$

$$\mathrm{OH + H_2 \rightarrow H_2O + H.} \quad (8)$$

The formation of H_2 on warm dust grains in the disk atmosphere (Equation (6)) is justified by the findings of Cazaux & Tielens (2002) who measure a moderate H_2 formation rate on warm (up to 900 K) dust grains. Further, H_2 molecules might form through gas-phase reactions (e.g., Glassgold et al. 2009):

$$\mathrm{H^- + H \rightarrow H_2 + \mathit{e}.} \quad (9)$$

The neutral–neutral reactions (Equations (7) and (8)) require high temperature to occur ($T > 300$ K). If H_2 is absent and hydrogen is mainly atomic, water may form through radiative association reactions (e.g., Kamp et al., submitted) such as

$$\mathrm{H + O \rightarrow OH + \mathit{h\nu}} \quad (10)$$

$$\mathrm{OH + H \rightarrow H_2O + \mathit{h\nu}.} \quad (11)$$

In both cases (neutral–neutral or radiative association reactions), the gas-phase formation of water in the disk atmosphere strongly depends on the gas density.

Recently, a number of stationary disk chemical models have shown that water can be efficiently formed in the warm disk surface layer. Glassgold et al. (2009, hereafter G09) investigated in situ water formation with a model based on X-ray (only) heating and ionization of the disk atmosphere which is most appropriate for T Tauri stars. Woitke et al. (2009, hereafter ProDiMo model) compute the thermo-chemical structure of Herbig AeBe disks which generally have $L_X/L_{\mathrm{FUV}} \ll 1$ (Kamp et al. 2008) using only UV/optical irradiation. According to their model there exists a hot water layer at distances between 1 and 30 AU and relative height $z/r \lesssim 0.1$–0.3 where water molecules are thermally decoupled from the dust ($T(\mathrm{H_2O}) > T(\mathrm{dust})$). In this model OH (and CO) are abundant within 30 AU of the star and above an A_V of a few where water is not efficiently formed. Water is only found in deeper layers where it is shielded from photodissociation and densities/temperatures are high enough to form it through neutral–neutral gas-phase chemistry.

5.2. Destruction of Water in Disks

PMSs emit strong ultraviolet radiation. For classical T Tauri stars, UV photons are produced by three main components: the

stellar photosphere, the enhanced chromospheric activity, and the magnetospheric accretion. In an X-ray irradiated T Tauri disk (as the one investigated by G09), water molecules are dissociated in the disk atmosphere through charge transfer reactions with H^+. In the case of early spectral type stars (B and A) as the ones studied here, the stellar photosphere is the major source of FUV radiation and overwhelms any contribution from mass accretion or stellar activity. The UV radiation field impinging onto the surface of the circumstellar disk affects the physical properties (such as the gas and dust temperature) of the disk as well as its chemistry. In the case of the OH/H_2O chemistry, the strength of the UV field regulates the formation/destruction rate. Due to the strong soft UV radiation, water can be easily photodissociated (e.g., Woitke et al. 2009):

$$H_2O + h\nu \rightarrow OH + H \quad (12)$$

$$\rightarrow O + 2H \quad (13)$$

$$\rightarrow O + H_2. \quad (14)$$

Water can also be destroyed by charge transfer reactions as in the case of T Tauri stars (e.g., G09). However, given the intense ultraviolet radiation, UV photodissociation is likely to be the major dissociation mechanism in the atmosphere of a Herbig Ae/Be star as we will show next.

The minimum energy required to dissociate water molecules is 5.1 eV (e.g., Harich et al. 2000) which corresponds to a radiation of $\lambda = 2430$ Å. The photodissociation cross section (k_{pd}) of water varies with the color of the impinging radiation field. As an example, the cross section for an incoming radiation of a 10,000 K blackbody is nearly four times larger that for a 4,000 K blackbody (van Dishoeck et al. 2008). This is due to the stronger soft UV radiation (relevant for the photodissociation of water molecules) of Herbig AeBe stars compared to T Tauri stars. Column 4 of Table 2 lists the UV luminosity of the program stars integrated between 1100 Å and 2430 Å. The integrated luminosity is multiplied by a factor of $10^{0.4 \cdot A_{1770}}$ to correct for interstellar extinction. The quantity A_{1770} is the extinction at $\lambda = 1770$ Å and it is measured from A_V using the $R = 3.1$ extinction relation of Cardelli et al. (1989). The UV luminosity of the program stars ranges between ~1 and 10^3 $L_\odot$. In the case of a classical T Tauri star, the UV luminosity ranges between ~0.01 and 1 $L_\odot$. In particular, for the two stars in Salyk et al. (2008; AS 205A, DR Tau) L_{UV} is ~0.1–1 $L_\odot$. Thus, the UV radiation emitted by the Herbig AeBe stars in this sample is up to 4 orders of magnitude larger than that in the T Tauri stars studied by Salyk et al. (2008). Photodissociation is a plausible mechanism to explain the lack of hot water vapor lines in Herbig AeBe disks.

A way to test this scenario further would be to detect OH rovibrational lines in the mid-infrared at high J rotational levels. In fact OH molecules formed by the photodissociation of water (Equation (12)) are vibrationally and rotationally excited (e.g., Dutuit et al. 1985; van Harrevelt & van Hemert 2000; Harich et al. 2000). As a consequence, the high rotational levels of OH are easily populated (e.g., Carrington 1964; Harich et al. 2000; Bonev & Mumma 2006) and mid-infrared spectra could be able to detect the high J-value transitions such as those found in the outflow of HH 211 (Tappe et al. 2009) and in TW Hya (Najita et al. 2010). A few high-J OH lines have been detected in the mid-infrared toward Herbig AeBe stars with disks (B. Sturm 2011, private communication). We note however that, depending on the density of the environment, the OH molecules might be thermalized very fast. This might prevent us from detecting any trace of water photodissociation. In this regard, the rotational diagram of L-band OH lines in the two stars studied by Mandell et al. (2008) is characterized by a single rotational temperature.

In addition to photodissociation, there are effects that could prevent us from detecting water vapor emission from the atmosphere of Herbig AeBe disks. The first effect to consider is the temperature difference between OH and H_2O lines detected here and in Salyk et al. (2008). The lower energy state of the OH P4.5 doublet is ~500 K while the energy state of H_2O transitions covered by our observations is $\gtrsim$1000 K. Thus, the OH emission potentially traces colder gas than the H_2O emission. One might speculate whether the H_2O non-detections are due to the different temperature layers probed in the disk. We find this possibility unlikely given that the OH transitions detected by Mandell et al. (2008) in AB Aur and MWC 758 have energies up to ~2360 K (OH P9.5), similar to the H_2O detected by Salyk et al. (2008). Thus, the high OH/H_2O line flux ratio in Herbig AeBe stars is a signature of water depletion in the disk atmosphere rather than of transitions tracing different temperatures.

Another argument that is often used to explain the paucity of molecular emission lines in Herbig AeBe disks is that the strong infrared excess might be able to veil the faint emission of molecular lines in the infrared (e.g., Pontoppidan et al. 2010). In this case, the molecular emission lines are veiled by the dust continuum. In this regard, we note that we detect OH emission at similar wavelengths and similar sensitivity of the H_2O rovibrational transitions detected in T Tauri disks. Thus, if water vapor is present, it must be located deeper in the disk (at higher A_V), where is colder than the OH detected here and/or thermally coupled with the dust (i.e., $T(H_2O) = T(\text{dust})$).

5.2.1. OH Photodissociation

The most probable photodissociation channel of water is the one that produces an OH molecule (~80%–90%, e.g., Crovisier 1989; Combi et al. 2004; Harich et al. 2000) that is followed by

$$OH + h\nu \rightarrow O + H. \quad (15)$$

The photodissociation cross section of H_2O is only twice as large as that of the OH for an incoming blackbody radiation of 10,000 K which is representative of a Herbig Ae star (van Dishoeck et al. 2008). In addition, the minimum energy needed to break the OH bond is 4.47 eV which corresponds to a radiation of 2616 Å (van Dishoeck & Dalgarno 1983), very similar to that of water. This suggests that OH molecules should also photodissociate as is seen in comets (e.g., Combi et al. 2004). The dissociation of OH by UV photons (Equation (15)) is thought to be the main reservoir of the excited oxygen (^{1}D) atoms which often produce the 6300 Å transition in solar system comets and in Herbig AeBe stars (e.g., van Dishoeck & Dalgarno 1984; Storzer & Hollenbach 1998; Morgenthaler et al. 2001; Acke et al. 2005).[15] The similar radial distributions of OH and [O I] in HD 259431 (Section 4 and Bagnoli et al. 2010) might be direct evidence of the formation of O(^{1}D) atoms via OH photodissociation.

The previous discussion suggests that the atmosphere of Herbig AeBe disks is depleted in water vapor. The detection of

[15] We note that another source of O(^{1}D) atoms is the direct photodissociation of water (Equation (14)).

OH emission and the column density ratio $OH/H_2O \gtrsim 1$ suggest that OH molecules are again produced in situ (Equation (7)).

5.3. Transport of Water in Disks

Non-stationary processes might affect the content of water in disks. Within a protoplanetary disk gas and solid particles can migrate either inward or outward (for a review see Ciesla & Cuzzi 2006) or can be mixed by, e.g., turbulent motions. Outward migration was suggested, e.g., by Stevenson & Lunine (1988), to explain the formation of Jupiter. Inward migration was studied by Ciesla & Cuzzi (2006) with the aim of addressing the abundance of hot water vapor found in some T Tauri stars. Water can form efficiently in the disk interior on the surface of dust grains. If water-rich bodies such as icy planetesimals migrate inward and pass the snow line, the water ice evaporates from their surface and enriches the inner disk of water vapor. For such a process to happen, however, the migration of planetesimals must be very fast and occur on a timescale shorter than the disk lifetime. Testing this hypothesis is important to probe the initial conditions of planetary systems. In this regard, two parameters are important: (1) the abundance of deuterated water and (2) the ortho–para ratio of water (e.g., Encrenaz 2008). Both these parameters are sensitive to the temperature of formation and hence to the region where water forms in the disk (atmosphere or disk interior). We invite the interested reader to look into the recent work of Thi et al. (2010) for a detailed theoretical treatment of the formation of deuterated water.

The case studied by Ciesla & Cuzzi (2006) is appropriate for T Tauri stars and does not include photodissociation. In the case of Herbig AeBe stars, however, the transport and/or mixing of volatiles might induce the depletion of water in the disk interior by dredging up molecules to the surface layers where molecules are photodissociated. Two timescales are important in this regard: (1) the chemical relaxation timescale ($\tau_{\rm chem}$) which regulates how fast chemical reactions occur and hence the formation of water, and (2) the mixing timescale. If the vertical mixing is faster than the chemical relaxation, the disk interior can be depleted of water. Estimates of $\tau_{\rm chem}$ for a Herbig Ae disk computed with ProDiMo are $\lesssim 10^2$ yr. The simulations of the transport processes in disks, e.g., by Ilgner et al. (2004), suggest that vertical mixing is slower and does not affect the global chemical evolution of the disk.

In this regard, ProDiMo predicts very different chemical structures between T Tauri and Herbig AeBe disks: T Tauri disks are colder and $\tau_{\rm chem}$ may be as long as 10^8 yr in the dense mid-plane where water is condensed in ice. Disks around Herbig AeBe stars instead have a hotter and more (chemically) active environment and there is only a very small amount of icy water in the mid-plane.

5.4. Gas–Dust Decoupling and Dust Settling

An important parameter for the photochemistry of disks is the physical decoupling of gas and dust in the disk atmosphere (e.g., Meijerink et al. 2009). Direct observational evidence of physical gas and dust decoupling was found for the Herbig Ae stars HD 101412 (Fedele et al. 2008) and HD 95881 (Verhoeff et al. 2010). In the case of physical decoupling, the disk atmosphere is depleted in large dust grains (which settle into the mid-plane) and water molecules are unshielded from the UV radiation. In such a case the molecular content in the disk atmosphere might be easily reduced by UV photodissociation. The situation changes dramatically if water and OH *self shielding* is taken into account as in Bethell & Bergin (2009). According to their model, in a dust-depleted disk atmosphere water and OH molecules become the major source of UV opacity and are able to block the photodissociative radiation from penetrating further into the disk. As a consequence, the abundance of water is enhanced even in the presence of moderate FUV radiation ($L_{\rm FUV} = 10\ L_{\odot}$). One problem with the water self-shielding model of Bethell & Bergin (2009) is that it assumes the presence of H_2 in the dust-depleted disk atmosphere. Without dust, however, H_2 forms via the H^- route which produces an overall lower abundance of molecular hydrogen. On the other hand, the model of Meijerink et al. (2009) as well as that of G09 and ProDiMo do not include water self-shielding. This makes it difficult to compare the observations with predictions from different models at this stage.

We do not have direct evidence of physical decoupling in the systems studied here but we do have evidence for thermal decoupling. If we assume a gas temperature of $T \sim 700$ K as found by Mandell et al. (2008) for AB Aur and MWC 758, the gas is hotter than the dust (T(dust) $\lesssim 300$ K, e.g., Kamp & Dullemond 2004) at a spatial scale of ∼1–20 AU, the size of the OH emitting region (Section 4). Thus, the OH vapor detected here is likely thermally decoupled from the dust.

5.5. OH Emission and Disk Geometry

In Section 4.1, we found that the presence of OH rovibrational lines correlates with the geometry of the disk: OH emission is mainly detected toward flaring disks (group I). As we saw in Section 3.1.1, the excitation of the OH rovibrational transitions depends on the temperature and density of the gas in the case of thermal emission and on the intensity of the UV and near-infrared radiation field in the case of fluorescence. In the case of Herbig AeBe stars the disk temperature is regulated by the UV output of the star as well as the near-infrared continuum emitted by the disk. Thus, the intensity of OH rovibrational lines depends on the UV radiation field impinging into the disk surface regardless of the excitation mechanism. In a flaring disk geometry, the disk surface area that is illuminated by the central star is much larger than in a self-shadowed geometry. In the latter case OH might still be excited but the emitting area is small (and the emission weak) and confined to the inner part of the disk.

A trend is also found between CO fundemantal rovibrational emission at 4.7 μm and disk flaring (G. van der Plas et al. 2011, submitted). CO emission originates from a larger disk area in flaring disks compared to flat disks. A larger sample of Herbig AeBe disks and more OH transitions are necessary to pin down the OH line excitation mechanism.

6. CONCLUSIONS

This paper presents high-resolution L-band spectroscopic observations of Herbig AeBe stars with disks. Of the 11 stars analyzed here, four show hot OH emission which appears to correlate with the disk geometry and, in turn, with the UV irradiation impinging on the disk. The detection rate of OH emission is 70% for disks with a flared geometry (including the two systems analyzed by Mandell et al. 2008) and ∼13% (1 out of 6) for self-shadowed disks. The OH rovibrational lines are spectrally resolved allowing us to measure an extension of ∼10–30 AU for the OH emitting region. In contrast to T Tauri, Herbig AeBe stars do not show evidence of hot water vapor in their spectra. The detections of OH emission lines and the observed OH/H_2O

column density ratio ($\gtrsim$1) indicate that the atmosphere of disks around Herbig AeBe stars is depleted in water molecules. Given the stronger UV radiation field of Herbig AeBe stars compared to T Tauri stars, a plausible explanation for the non-detection of water lines is that water in the disk atmosphere is dissociated by UV photons. The absence of hot water vapor in the disk atmosphere does not preclude the existence of colder water deeper in the disk (at lower temperature and higher A_V). Far-infrared water lines have been detected with the *Herschel Space Observatory* toward the Herbig Ae star HD 100546 (Sturm et al. 2010) (although further confirmation is needed). This indicates the presence of warm water vapor in the disk.

D. Fedele thanks B. Acke for kindly providing the IDL script "keprot" used in the analysis. D.F. thanks A. Carmona, G. van der Plas, M. E. van den Ancker, A. M. Mandell, D. Neufeld, and C. P. Dullemond for useful discussion and suggestions. We are grateful to the ESO staff in Garching and at Paranal for performing the CRIRES observations in service mode. D.F. is supported by an NSF Astronomy & Astrophysics research grant to IP (ID: AST0908479). We thank the anonymous referee for helpful comments.

Facilities: VLT:Antu

APPENDIX

ON THE ASYMMETRIC OH LINE PROFILE IN V380 ORI

As we saw in Section 4.2, the OH line profile in V380 Ori is asymmetric, with the blueshifted component brighter than the redshifted one. A similar asymmetry was found toward other protoplanetary disks in the [O I] 6300 Å line for the Herbig Ae star HD 100546 (Acke & van den Ancker 2006) and in the CO fundamental rovibrational lines in EX Lupi (Goto et al. 2011). Such an asymmetry is either due to a deviation from the Keplerian motion of the gas or to a non-homogeneous distribution of the emitting gas. The inner radius of the OH emitting region ($\sim$2 AU) is too large to be coincident with the dust sublimation radius. Alecian et al. (2009) found evidence of a close low-mass star companion to V380 Ori. They determine a projected angular separation $a \sin(i) < 0.33$ AU. Regardless of the inclination, the orbit of the companion is certainly within the inner rim of the OH emitting region. Circumbinary disks have inner gap of the order of $\sim$2–3 times the binary separation (Artymowicz & Lubow 1994) which brings the truncation radius to $\sim$1–2 AU for V380 Ori (depending on the eccentricity, inclination, and mass ratio of the binary). This is remarkably close to the OH inner radius estimated here. The companion might also be the source of the perturbation of the gas dynamics seen in the OH line profile. Recent simulation by Regály et al. (2011) show that in the case of a circumbinary disk the velocity distribution of the gas differs from the circular Keplerian case. The disk may become eccentric (due to tidal interaction with the lower-mass companion) and the velocity profile of the emerging lines is asymmetric in a fashion similar to Figure 2.

REFERENCES

Acke, B., & van den Ancker, M. E. 2006, A&A, 449, 267
Acke, B., van den Ancker, M. E., & Dullemond, C. P. 2005, A&A, 436, 209
Alecian, E., et al. 2009, MNRAS, 400, 354
Artymowicz, P., & Lubow, S. H. 1994, ApJ, 421, 651
Bagnoli, T., van Lieshout, R., Waters, L. B. F. M., van der Plas, G., Acke, B., van Winckel, H., Raskin, G., & Meerburg, P. D. 2010, ApJ, 724, L5
Barber, R. J., Tennyson, J., Harris, G. J., & Tolchenov, R. N. 2006, MNRAS, 368, 1087
Bethell, T., & Bergin, E. 2009, Science, 326, 1675
Blum, J., & Wurm, G. 2008, ARA&A, 46, 21
Bonev, B. P., & Mumma, M. J. 2006, ApJ, 653, 788
Bouret, J., Martin, C., Deleuil, M., Simon, T., & Catala, C. 2003, A&A, 410, 175
Bouwman, J., Lawson, W. A., Dominik, C., Feigelson, E. D., Henning, T., Tielens, A. G. G. M., & Waters, L. B. F. M. 2006, ApJ, 653, L57
Bouwman, J., Meeus, G., de Koter, A., Hony, S., Dominik, C., & Waters, L. B. F. M. 2001, A&A, 375, 950
Brittain, S. D., Rettig, T. W., Simon, T., Kulesa, C., DiSanti, M. A., & Dello Russo, N. 2003, ApJ, 588, 535
Brittain, S. D., Simon, T., Najita, J. R., & Rettig, T. W. 2007, ApJ, 659, 685
Calvet, N., Muzerolle, J., Briceño, C., Hernández, J., Hartmann, L., Saucedo, J. L., & Gordon, K. D. 2004, AJ, 128, 1294
Cardelli, J. A., Clayton, G. C., & Mathis, J. S. 1989, ApJ, 345, 245
Carmona, A., van den Ancker, M. E., Henning, T., Goto, M., Fedele, D., & Stecklum, B. 2007, A&A, 476, 853
Carr, J. S., & Najita, J. R. 2008, Science, 319, 1504
Carr, J. S., Tokunaga, A. T., & Najita, J. 2004, ApJ, 603, 213
Carrington, T. 1964, J. Chem. Phys., 41, 2012
Cazaux, S., & Tielens, A. G. G. M. 2002, ApJ, 575, L29
Ciesla, F. J., & Cuzzi, J. N. 2006, Icarus, 181, 178
Combi, M. R., Harris, W. M., & Smyth, W. H. 2004, in Comets II, ed. M. C. Festou, H. U. Keller, & H. A. Weaver (Tucson, AZ: Univ. Arizona Press), 523
Crovisier, J. 1989, A&A, 213, 459
de Winter, D., & van den Ancker, M. E. 1997, A&AS, 121, 275
de Winter, D., van den Ancker, M. E., Maira, A., Thé, P. S., Djie, H. R. E. T. A., Redondo, I., Eiroa, C., & Molster, F. J. 2001, A&A, 380, 609
Dello Russo, N., Bonev, B. P., DiSanti, M. A., Mumma, M. J., Gibb, E. L., Magee-Sauer, K., Barber, R. J., & Tennyson, J. 2005, ApJ, 621, 537
Dello Russo, N., Disanti, M. A., Magee-Sauer, K., Gibb, E. L., Mumma, M. J., Barber, R. J., & Tennyson, J. 2004, Icarus, 168, 186
Dullemond, C. P., & Dominik, C. 2004, A&A, 417, 159
Dutuit, O., Tabche-Fouhaile, A., Nenner, I., Frohlich, H., & Guyon, P. M. 1985, J. Chem. Phys., 83, 584
Encrenaz, T. 2008, ARA&A, 46, 57
Fedele, D., van den Ancker, M. E., Henning, T., Jayawardhana, R., & Oliveira, J. M. 2010, A&A, 510, A72
Fedele, D., et al. 2008, A&A, 491, 809
Garcia Lopez, R., Natta, A., Testi, L., & Habart, E. 2006, A&A, 459, 837
Glassgold, A. E., Meijerink, R., & Najita, J. R. 2009, ApJ, 701, 142
Goto, M., et al. 2011, ApJ, 728, 5
Haisch, K. E., Jr., Lada, E. A., & Lada, C. J. 2001, ApJ, 553, L153
Harich, S. A., Hwang, D. W. H., Yang, X., Lin, J. J., Yang, X., & Dixon, R. N. 2000, J. Chem. Phys., 113, 10073
Henning, T., Dullemond, C. P., Wolf, S., & Dominik, C. 2006, in Planet Formation, ed. H. Klahr & W. Brandner (Cambridge: Cambridge Univ. Press), 112
Hernández, J., Calvet, N., Briceño, C., Hartmann, L., & Berlind, P. 2004, AJ, 127, 1682
Hernández, J., et al. 2007, ApJ, 662, 1067
Herzberg, G. 1950, Molecular Spectra and Molecular Structure. Vol. 1: Spectra of Diatomic Molecules (2nd ed.; New York: Van Nostrand Reinhold)
Hillenbrand, L. A., Strom, S. E., Vrba, F. J., & Keene, J. 1992, ApJ, 397, 613
Horne, K., & Marsh, T. R. 1986, MNRAS, 218, 761
Hubrig, S., et al. 2009, A&A, 502, 283
Ilgner, M., Henning, T., Markwick, A. J., & Millar, T. J. 2004, A&A, 415, 643
Ingleby, L., et al. 2009, ApJ, 703, L137
Jayawardhana, R., Coffey, J., Scholz, A., Brandeker, A., & van Kerkwijk, M. H. 2006, ApJ, 648, 1206
Kaeufl, H., et al. 2004, Proc. SPIE, 5492, 1218
Kamp, I., & Dullemond, C. P. 2004, ApJ, 615, 991
Kamp, I., Freudling, W., Robberto, M., Chengalur, J., & Keto, E. 2008, Phys. Scr. T, 130, 014013
Kennedy, G. M., & Kenyon, S. J. 2008, ApJ, 682, 1264
Kraus, S., Preibisch, T., & Ohnaka, K. 2008, ApJ, 676, 490
Kurucz, R. L. 1979, ApJS, 40, 1
Malfait, K., Bogaert, E., & Waelkens, C. 1998, A&A, 331, 211
Mandell, A. M., Mumma, M. J., Blake, G. A., Bonev, B. P., Villanueva, G. L., & Salyk, C. 2008, ApJ, 681, L25
Manoj, P., Bhatt, H. C., Maheswar, G., & Muneer, S. 2006, ApJ, 653, 657
Martin-Zaïdi, C., et al. 2008, A&A, 484, 225
Meeus, G., Waters, L. B. F. M., Bouwman, J., van den Ancker, M. E., Waelkens, C., & Malfait, K. 2001, A&A, 365, 476

Meijerink, R., Pontoppidan, K. M., Blake, G. A., Poelman, D. R., & Dullemond, C. P. 2009, ApJ, 704, 1471
Merín, B., et al. 2004, A&A, 419, 301
Mohanty, S., Jayawardhana, R., & Basri, G. 2005, ApJ, 626, 498
Montesinos, B., Eiroa, C., Mora, A., & Merín, B. 2009, A&A, 495, 901
Morel, M., & Magnenat, P. 1978, A&AS, 34, 477
Morgenthaler, J. P., et al. 2001, ApJ, 563, 451
Najita, J. R., Carr, J. S., Strom, S. E., Watson, D. M., Pascucci, I., Hollenbach, D., Gorti, U., & Keller, L. 2010, ApJ, 712, 274
Pascucci, I., & Tachibana, S. 2010, in Protoplanetary Dust, ed. D. A. Apai & D. S. Lauretta (Cambridge: Cambridge Univ. Press), 263
Podolak, M. 2010, in IAU Symp. 263, Icy Bodies in the Solar System, ed. J. A. Fernández, D. Lazzaro, D. Prialnik, & R. Schulz (Cambridge: Cambridge Univ. Press), 19
Pontoppidan, K. M., Salyk, C., Blake, G. A., Meijerink, R., Carr, J. S., & Najita, J. 2010, ApJ, 720, 887
Regály, Z., Sándor, Z., Dullemond, C. P., & Kiss, L. L. 2011, A&A, 528, A93
Roccatagliata, V., Henning, T., Wolf, S., Rodmann, J., Corder, S., Carpenter, J. M., Meyer, M. R., & Dowell, D. 2009, A&A, 497, 409
Rodmann, J., Henning, T., Chandler, C. J., Mundy, L. G., & Wilner, D. J. 2006, A&A, 446, 211
Rothman, L. S., et al. 2009, J. Quant. Spectrosc. Radiat. Transfer, 110, 533
Salyk, C., Pontoppidan, K. M., Blake, G. A., Lahuis, F., van Dishoeck, E. F., & Evans, N. J., II 2008, ApJ, 676, L49
Sicilia-Aguilar, A., Hartmann, L. W., Fürész, G., Henning, T., Dullemond, C., & Brandner, W. 2006, AJ, 132, 2135
Smak, J. 1981, Acta Astron., 31, 395
Stevenson, D. J., & Lunine, J. I. 1988, Icarus, 75, 146
Storzer, H., & Hollenbach, D. 1998, ApJ, 502, L71
Sturm, B., et al. 2010, A&A, 518, L129
Tappe, A., Lada, C. J., Black, J. H., & Muench, A. A. 2009, in The Evolving ISM in the Milky Way and Nearby Galaxies, Proc. 4th Spitzer Science Center Conf., ed. K. Sheth, A. Noriega-Crespo, J. Ingalls, & R. Paladini, http://ssc.spitzer.caltech.edu/mtgs/ismevol/
Thi, W., & Bik, A. 2005, A&A, 438, 557
Thi, W., et al. 2010, A&A, 518, L125
Valenti, J. A., Fallon, A. A., & Johns-Krull, C. M. 2003, ApJS, 147, 305
van Boekel, R., Waters, L. B. F. M., Dominik, C., Bouwman, J., de Koter, A., Dullemond, C. P., & Paresce, F. 2003, A&A, 400, L21
van den Ancker, M. E., de Winter, D., & Tjin A Djie, H. R. E. 1998, A&A, 330, 145
van der Plas, G., van den Ancker, M. E., Acke, B., Carmona, A., Dominik, C., Fedele, D., & Waters, L. B. F. M. 2009, A&A, 500, 1137
van Dishoeck, E. F., & Dalgarno, A. 1983, J. Chem. Phys., 79, 873
van Dishoeck, E. F., & Dalgarno, A. 1984, Icarus, 59, 305
van Dishoeck, E. F., Jonkheid, B., & van Hemert, M. C. 2008, arXiv:0806.0088
van Harrevelt, R., & van Hemert, M. C. 2000, J. Chem. Phys., 112, 5777
van Kempen, T. A., et al. 2010, A&A, 518, L128
Verhoeff, A. P., et al. 2010, A&A, 516, A48
Weidenschilling, S. J., & Cuzzi, J. N. 1993, in Protostars and Planets III, ed. E. H. Levy & J. I. Lunine (Tucson, AZ: Univ. Arizona Press), 1031
Woitke, P., Kamp, I., & Thi, W. 2009, A&A, 501, 383